Nonlinear resonances of particles in a dusty plasma sheath

C. Zafiu, A. Melzer, and A. Piel
Institut für Experimentelle und Angewandte Physik, Christian-Albrechts-Universität Kiel, 24098 Kiel, Germany
(Received 5 December 2000; published 23 May 2001)

Vertical oscillations of microparticles trapped in the sheath of a capacitive rf discharge have been excited showing a strongly nonlinear resonance. The nonlinear oscillations are analyzed in terms of an anharmonic fourth-order potential energy curve. It is demonstrated that the observed nonlinearities can be related to a position dependent charge of the microspheres, whereas the electric field is found to be as nearly linearly increasing. The experimental results on the position dependent charging and electric field structure are compared to a numerical model.

DOI: 10.1103/PhysRevE.63.066403 PACS number(s): 52.27.Lw, 52.35.Fp

I. INTRODUCTION

In the last few years, dusty plasmas have attained a great interest because of their importance for astrophysical phenomena and their application in plasma processing technologies. Plasmas containing small particles (nanometer to micrometer size) are found in planetary rings, comets, nebulae, noctilucent clouds, etc. Dusty plasmas play an important role in industrial devices for microchip processing, where particle formation poses a serious problem of contamination. Technological applications are found in discharges with reactive gases for particle growth and deposition, as well as manufacturing of nanopowders, solar cells, and new materials.

Even more fascinating in view of fundamental physics is the observation that microspheres trapped in the plasma sheath form nearly two-dimensional crystal-like structures (the so called plasma crystals [1–4]) providing an ideal model for condensed matter on a macroscopic scale.

The charge of the grains and the electric field structure in the sheath are considered to be crucial parameters for the particle trapping and crystallization of microparticle crystals in laboratory experiments on Earth.

Oscillatory motion of particles that are trapped in the sheath of an rf discharge was already used as a diagnostic means for determining the charge on microspheres [5]. This technique was later refined by using a laser force on the particle [6], confirming the Q/M values found earlier. The various oscillation modes of a particle trapped in the sheath, including parametric excitation of the vertical resonance, were studied in Ref. [7].

Damped linear oscillations of particles dropped into the sheath were exploited to obtain a detailed insight into the particle charge [8]. The key point in all these experiments is that the electric field is considered to be linearly increasing and the charge on the particle is constant, resulting in a linear resonance of the oscillating particle. A linear resonance is characteristic of a particle oscillating in a parabolic effective potential well, that results from the assumptions on the electric field and particle charge [5,6,9].

Recently, the nonlinear oscillations of single particles, that were trapped into the sheath region were used to explore the electric field structure of the sheath [10]. Self-excited oscillations driven by a delayed charging due to a finite charging time were observed by Nunomura *et al.* [11].

In the experiments here, micrometer sized spherical plastic particles of three different sizes are trapped in the ionic space charge sheath of a capacitive rf discharge (see Sec. IV) and their vertical nonlinear oscillations are studied here to derive the position dependent charging. The experimental results are compared with a numerical model.

II. OSCILLATION MODEL

The particles trapped in the positive ionic space charge of an rf discharge, usually attain a high negative charge (see also Sec. III) due to the higher electron mobility. The resulting electric force on the particle points upwards against the gravitational force and the static equilibrium of the particle in the sheath is described by the force balance [see Fig. 1(b)]

$$Mg = Q(x)E(x). \tag{1}$$

Here, we assume that the charge and electric field are position dependent but time averaged. x is coordinate in the ''local coordinate system'' relative to the particle equilibrium position. The ''absolute coordinate system'' is taken to be relative to the sheath edge. With x_0 being the equilibrium particle position in the 'absolute'' system, $x + x_0 = X$.

The general equation of motion then has the form

$$M\ddot{x} + M\beta\dot{x} = Q(x)E(x) - Mg + F_{exc}\sin(\omega t). \tag{2}$$

$M\beta\dot{x}$ is the force due to the friction of the particle with the neutrals [12]. The excitation force $F_{exc}\sin(\omega t)$ is due to the modulation of the rf power with a low frequency voltage, that results in a ''shaking'' of the plasma sheath with the applied low frequency. This periodical force drives the particle oscillation.

Other forces like the thermophoretic force [5], and the ion drag force [9] are neglected here. They are commonly assumed to be much smaller than the electric field force or gravity in the sheath, for large dust grains ($\geqslant 2\ \mu$m).

In previous experiments [5,9], the electric field was assumed as linearly increasing from the sheath edge to the electrode [see Fig. 1(b)]; it was also assumed that the electric charge on the dust grains is constant over the regions covered by the oscillations. This results in a parabolic effective potential energy well for the particle. In this case, the general equation of motion simplifies to

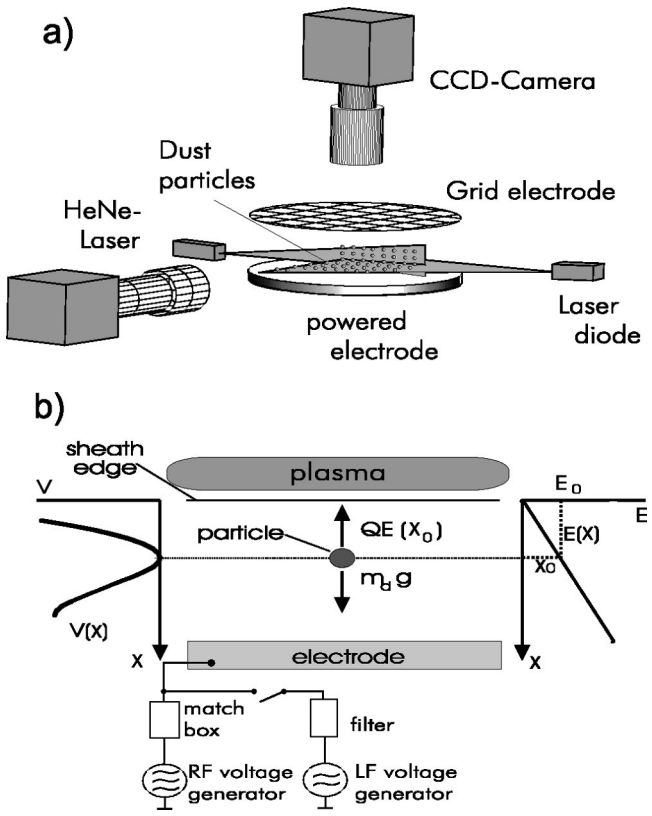

FIG. 1. Scheme of the experimental setup (a) and equilibrium in the sheath, modulation technique, electric field, and effective potential (b).

$$\ddot{x}+\beta\dot{x}+\omega_0^2 x=\frac{1}{M}F_{exc} \tag{3}$$

with $\omega_0^2=Q_0E_1$, where Q_0 is the constant charge and E_1 is the slope of the electric field. This equation describes a damped harmonic oscillation with a linear resonance. Such linear resonances of single particles were exploited to measure the electric charge of the dust grains [5].

Variation of the electron and ion densities and currents in the sheath lead to a deviation from the linearly increasing electric field profile and to a position-dependent dust charge. This results in a nonparabolic effective potential energy well that the particle experiences. In our analysis it is assumed that the electric field and the charge are described by polynomial functions

$$\begin{aligned} Q(x)&=Q_0+Q_1x+Q_2x^2+Q_3x^3\\ &=\tilde{Q}_0+\tilde{Q}_1X+\tilde{Q}_2X^2+\tilde{Q}_3X^3, \end{aligned} \tag{4}$$

$$\begin{aligned} E(x)&=E_0+E_1x+E_2x^2+E_3x^3\\ &=\tilde{E}_0+\tilde{E}_1X+\tilde{E}_2X^2+\tilde{E}_3X^3. \end{aligned} \tag{5}$$

[$\tilde{E}_0=0$ since $E(X)=0$ at the sheath edge $X=0$.] The equation of motion then becomes nonlinear, including higher order terms

$$\ddot{x}+\beta\dot{x}+C_1x+C_2x^2+C_3x^3+\cdots=\frac{F_{exc}}{M}\cos(\omega t). \tag{6}$$

The coefficients C_1, C_2, and C_3 are combinations of electric field and charge coefficients.

$$C_1=\frac{1}{M}(Q_0E_1+Q_1E_0), \tag{7}$$

$$C_2=\frac{1}{M}(Q_0E_2+Q_1E_1+Q_2E_0), \tag{8}$$

$$C_3=\frac{1}{M}(Q_0E_3+Q_1E_2+Q_2E_1+Q_3E_0). \tag{9}$$

C_2 and C_3 describe the nonlinear terms giving the deviation of the effective potential energy well from the simple parabolic shape. If C_2 and C_3 are zero, then the simple damped harmonic oscillation is obtained, with the frequency determined by C_1. C_2 determines the up/down asymmetry of the potential in the sheath and C_3 determines the weakening or strengthening of the potential energy well for higher oscillation amplitudes.

Higher orders that could be taken into account in the equation of motion would add new unknown coefficients. Here we restrict ourselves to the three coefficients holding the main information, i.e., resonance frequency (C_1), oscillation/potential asymmetry (C_2), and weakening/strengthening of the potential (C_3).

III. CHARGING AND SHEATH MODEL

The experiments are compared with a model of particle charging in the sheath of an rf discharge to give a more detailed insight into the problem.

Here, the particle charging is described by the commonly used OML model. Because of their large size compared to the plasma components (ions and electrons) the dust particles act like small probes collecting ionic and electronic currents on their surface. In the special situation of the sheath, a modified expression for the ion current, that accounts for the supersonic ion flow in the sheath is adopted [13]

$$I_i(\Phi_p,x_p)=n_se\pi R^2\left(\frac{k_BT_e}{m_i}\right)^{1/2}\left[1-2\frac{e\Phi_p}{k_BT_e}\left(\frac{v_B}{v_i(x_p)}\right)^2\right], \tag{10}$$

$$I_e(\Phi_p,x_p)=-n_e(x_p)e\pi R^2\left(\frac{8k_BT_e}{\pi m_e}\right)^{1/2}\exp\left(\frac{e\Phi_p}{k_BT_e}\right). \tag{11}$$

Here R is the particle radius, k_B is the Boltzmann constant, m_i and m_e are the ion and electron mass respectively, T_e is the electron temperature, and Φ_p the surface potential of the particle relative to the local plasma potential at the particle position. In the sheath, the reduced electron density is taken into account for the electron current. Therefore n_e is the electron density at the particle position x_p. The ions are assumed to be accelerated to the velocity v_i by the sheath

electric field without collisions. The ion density at the particle position can then be determined, according to the equation of continuity

$$n_i(x_p)v_i(x_p)=n_s v_B, \tag{12}$$

where n_s is the ion/electron density at the sheath edge and v_B is the Bohm velocity. The electron and ion currents are therefore position dependent due to the reduction of the electron density and increase of ion velocity in the sheath, respectively. n_e and v_i are taken as position dependent but time averaged values over the rf period because the rf period is much smaller than the charging time or the oscillation period of the dust particle.

The equilibrium floating potential and thus the equilibrium charge are derived from the balance of the electron and ion currents. The charge on the particulate is related to the floating potential, assuming the particle as a spherical capacitor [5]

$$C=4\pi\varepsilon_0 R, \tag{13}$$

$$Q=C\Phi_p. \tag{14}$$

The sheath model of Lieberman [14] is applied here to calculate the electron and ion densities, velocities, and electric field in the sheath.

The sheath model of Lieberman [14] presents a self-consistent solution for the ion and electron densities and the electric potential in the sheath, obtained under the assumptions of time independent, collisionless ion motion, and inertialess electrons. Using the model of Lieberman, the electric field, ion and electron densities, and floating potential on the grain surface have been calculated and plotted in the absolute coordinate system in Fig. 2.

Multiplying the calculated charge $Q(x)$ with the electric field $E(x)$, the potential energy curve is obtained after integration. This calculated potential curve was compared with the potential determined from the experimental values using C_1, C_2, and C_3 [see Sec. V and Fig. 3(b)].

Figure 2(c) represents the calculated electric field in the sheath, together with a linear fit. As it can be observed, the electric field is almost linear over the whole plasma sheath, in agreement with recent results [15]. Only in the vicinity of the plasma edge, the electric field starts with a smaller slope. To simplify the analysis of the experiment, we assumed the following approximation for the electric field: at the sheath edge ($X=0$), it starts as zero until the ''turning point'' (at $X=x_s$) from which on the field continues as a linearly increasing function [see Fig. 2(b), dotted curve].

Considering this, Eq. (5) becomes

$$E(X)=\begin{cases}0, & X\leqslant x_s\\ \tilde{E}_1(X-x_s)=E_0+E_1x, & X>x_s.\end{cases} \tag{15}$$

If this expression is replaced in the equations for C_1, C_2, and C_3, Eqs. (7), (8), and (9) become

$$C_1=\frac{1}{M}(Q_0E_1+Q_1E_0), \tag{16}$$

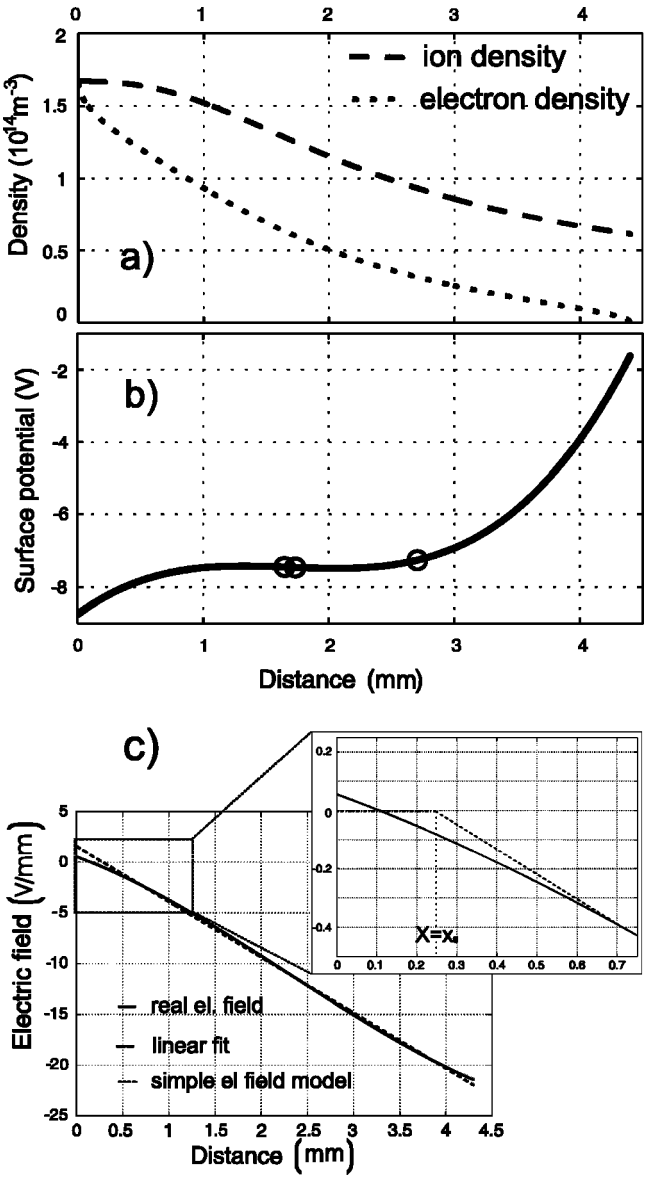

FIG. 2. Lieberman and Lichtenberg model; electron and ion densities (a), floating potential (b), and electric field (c). The symbols mark the positions where the the force balance is fulfilled for each particle.

$$C_2=\frac{1}{M}(Q_1E_1+Q_2E_0), \tag{17}$$

$$C_3=\frac{1}{M}(Q_2E_1+Q_3E_0), \tag{18}$$

where $E_0=E_1(x_0-x_s)$ with x_0 the equilibrium position of the particle. C_1, C_2, and C_3 are zero for $X\leqslant x_s$.

Assuming that the charging process is the same for all three particles, it is reasonable to introduce a ''charging function'' $\Phi_p(X)$. Under the assumption of the spherical capacitor charging model for the dust grains, this charging function is the floating potential. Therefore we split the

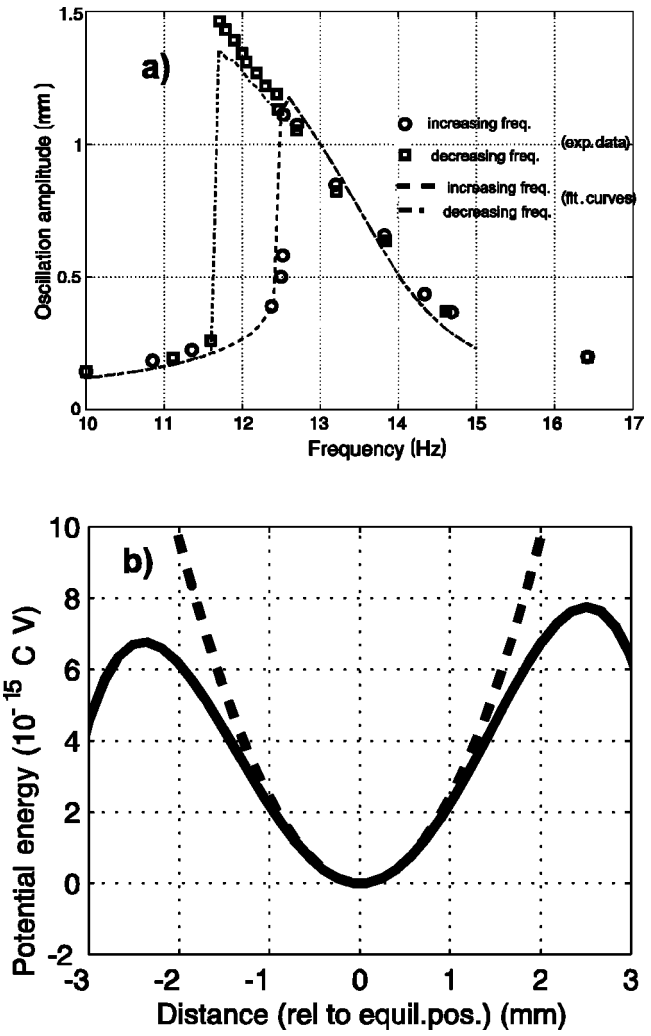

FIG. 3. Best-fit results of the nonlinear resonance curve (a) and effective potential well (b) for 9.47 μm particle. The dashed line in plot (b) represents the ideal parabolic potential well.

charge of the grain into the geometrical factor $4\pi\epsilon_0 R$ and assume the charging function as the ''universal'' floating potential $\Phi_p(X)$

$$Q(X)=\Phi_p(X)4\pi\epsilon_0 R. \tag{19}$$

The charging function is also assumed to be a third-order polynomial function of position, like the particle charge (see Eq. 4).

$$\Phi_p(X)=\tilde{\Phi}_0+\tilde{\Phi}_1 X+\tilde{\Phi}_2 X^2+\tilde{\Phi}_3 X^3 \tag{20}$$

Figure 2(b) shows the floating potential computed from balancing the electron and ion currents on the particle surface, according to Eqs. (10) and (11) and introducing the ion and electron average densities [plotted in Fig. 2(a)]. The open circles indicate the equilibrium positions for the three different particles with diameters of 9.47 μm, 12.07 μm, and 20.02 μm used in the experiments.

IV. EXPERIMENT

The experiments have been performed in a parallel plate rf discharge in helium at low pressure (5.8 Pa) and rf power of 13 W [see Fig. 1(a)]. Monodisperse, spherical plastic particles of 9.47 μm and 12.07 μm diameter, made of melamine formaldehyde, and of 20.02 μm diameter, made of polymethylmethacrylate are immersed into the plasma. The lower electrode is powered while the rest of the discharge chamber is grounded. The particles are trapped in the sheath above the lower electrode. Here, an electrode with a shallow parabolic trough is used to impose a very weak horizontal confinement on the particle. Two 690-nm laser diodes were used to illuminate the particles trapped in the sheath. One beam is expanded horizontally and the other vertically.

Two video cameras were used for observation from top and from side. The vertical laser sheet together with the side view camera are used to record images of the oscillating particle. The side view high speed camera allows recording at up to 200 frames/s.

Low frequency modulation of the rf voltage was used for excitation of large amplitude particle oscillation. By comparison with laser excitation, this voltage modulation technique has been shown not to affect the plasma environment [6]. The excitation signal is applied to the electrode through a low pass filter [see Fig. 1(b)]. The excitation amplitudes were: 5 V_{pp} (d=9.47 μm), 10 V_{pp} (d=12.07 μm), and 23 V_{pp} (d=20.02 μm). The oscillations are recorded over several oscillation periods, with up to 100 frames/s.

The three different particle sizes were used to inspect a large region of the sheath.

Very small particles of 0.93 μm were introduced to mark the position of the sheath edge ($X=0$). Because of their small mass, we assumed that they need a very small electric field to levitate them and, thus, we consider them lying at the sheath edge.

V. DATA PROCESSING TECHNIQUE AND RESULTS

The nonlinear resonance curves are measured in the following way. A single particle of one of the three different sizes is introduced into the chamber. The particle is trapped in the sheath of the lower electrode and then the low-frequency modulation is applied with various frequencies. The resulting oscillation amplitudes are measured upwards and downwards relative to the equilibrium position. The resulting resonance curves are shown in Fig. 4 for the smallest (9.47 μm) and the largest (20.02 μm) particle [12]. In our experiments, hysteretic resonance curves were obtained, that bend towards lower frequencies and yield jumps or drops in amplitude for increasing or decreasing frequency, respectively (see Fig. 4). The observed hysteresis is a general feature of nonlinear resonances [16]. From this overall behavior, it can already be deduced that the effective potential becomes softer with increasing the amplitude, that means that C_3 must be negative.

It is also easily observed that the oscillation is asymmetric and that the asymmetry depends on the position in the sheath. For the lighter particle (that oscillates close to the

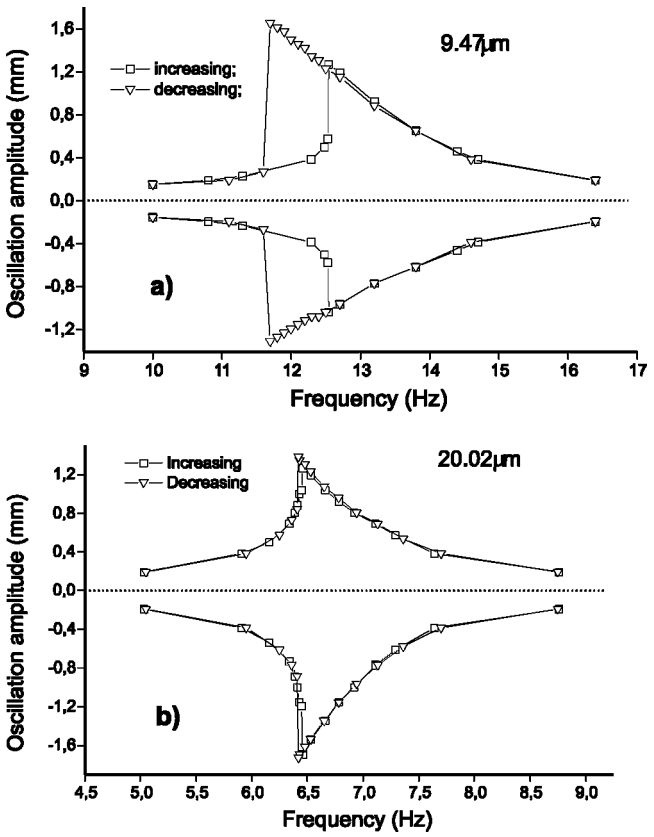

FIG. 4. Measured upwards and downwards amplitude curves for a 9.47 μm (a) and a 20.02 μm (b) particle, for increasing and decreasing frequency, relative to the equilibrium position.

sheath edge), the oscillation asymmetry is towards the plasma edge, which means a positive C_2. In the case of heavier particles (that oscillate deeper in the sheath), the oscillation asymmetry changes, showing a potential asymmetry towards the electrode, which means that C_2 is now negative.

The coefficients of nonlinearity C_1, C_2, and C_3 have been determined in two ways from the resonance curves. First, the equation of motion (6) is solved approximately, using the following trial solution [16]

$$x(t)=B_0+A_1\sin(\omega t)+B_1\cos(\omega t). \tag{21}$$

where B_0 is the term that defines the asymmetry (offset) of the oscillation. Considering that $A_1^2+B_1^2=D^2$, where D is the amplitude of oscillation, the general equation of motion can be solved, neglecting terms of higher harmonics ($\geqslant\omega$). The amplitude and the asymmetry of the oscillation are then obtained from the system

$$\left(\frac{F_{exc}}{M}\right)^2=\left[\omega^2-C_1-2C_2B_0-\frac{3}{2}C_3(2B_0^2+D^2)\right]^2D^2+\beta^2\omega^2D^2,$$

$$0=C_1B_0+\frac{1}{2}C_2(2B_0^2+D^2)+\frac{1}{4}C_3B_0(4B_0^2+3D^2)+g. \tag{22}$$

TABLE I. Best-fit values for coefficients C_1, C_2, and C_3.

d (μm)	C_1 (s^{-2})	C_2 ($m^{-1}s^{-2}$)	C_3 ($m^{-2}s^{-2}$)
9.47	7200	1.5×10^5	-1.2×10^9
12.07	6200	1×10^5	-1.1×10^9
20.02	1900	-5.1×10^5	-6×10^7

Solving this system for given C_1, C_2, and C_3, the nonlinear resonance curve can be calculated (D as a function of frequency). The damping constants, β were computed for each particle size used in the experiment [12]. They were found to be $\beta=1.64\,s^{-1}$ (9.47 μm), $1.28\,s^{-1}$ (12.07 μm), and $0.78\,s^{-1}$ (20.02 μm).

The second way of finding the values for C_1, C_2, and C_3 is by numerically solving the general equation of motion. This method is more general since we can take into account that the particle might be pushed into the plasma region where only the gravitation and friction forces act on it. Again, the values for the coefficients governing the equation of motion are obtained by fitting the computed resonance curve to the experimental one. The values found in this way are very close to those computed using the previous method. The differences are within 5% of each value.

Here, the numerical solution of the general equation of motion is used to find the best-fit values for C_1, C_2, and C_3. Figure 3(a) presents the best-fit result for the 9.47 μm particle (the averaged amplitude between the upwards and downwards excursions). Table I shows the best-fit values for the three coefficients for all three particle sizes.

As expected, the change of sign for C_2 (that defines the asymmetry of the effective potential well, see Fig. 3(b) in the case of 20.02 μm particle reflects the change of oscillation asymmetry experimentally observed. Also negative values of C_3 (related to the softening of the effective potential well) for all particle sizes were obtained, in agreement with the model.

At this point the coefficients in the equation governing the nonlinear oscillations of the particles have been derived. The aim is furthermore to see how the charging process and the electric field structure influence the effective potential, leading to the nonlinear features of the resonance curves that were discussed above (bending and asymmetry) and which are the nonlinear individual contributions either of the electric field and charge to the nonparabolic potential well.

Considering that the small particles of 0.93 μm lie just at the sheath edge, the electric field is chosen to be of the form described by Eq. (15) and the particle charge is defined by

$$\begin{aligned}Q(X)&=\tilde{Q}_0+\tilde{Q}_1X+\tilde{Q}_2X^2+\tilde{Q}_3X^3\\&=\tilde{Q}_0+\tilde{Q}_1(x+x_0)+\tilde{Q}_2(x+x_0)^2+\tilde{Q}_3(x+x_0)^3.\end{aligned} \tag{23}$$

x_0 is the position of the particle for which the resonance curve is recorded relative to the sheath edge, x_s is the distance from the sheath edge to the ''turning point'' where the electric field becomes linear and x is the ''local coordinate.''

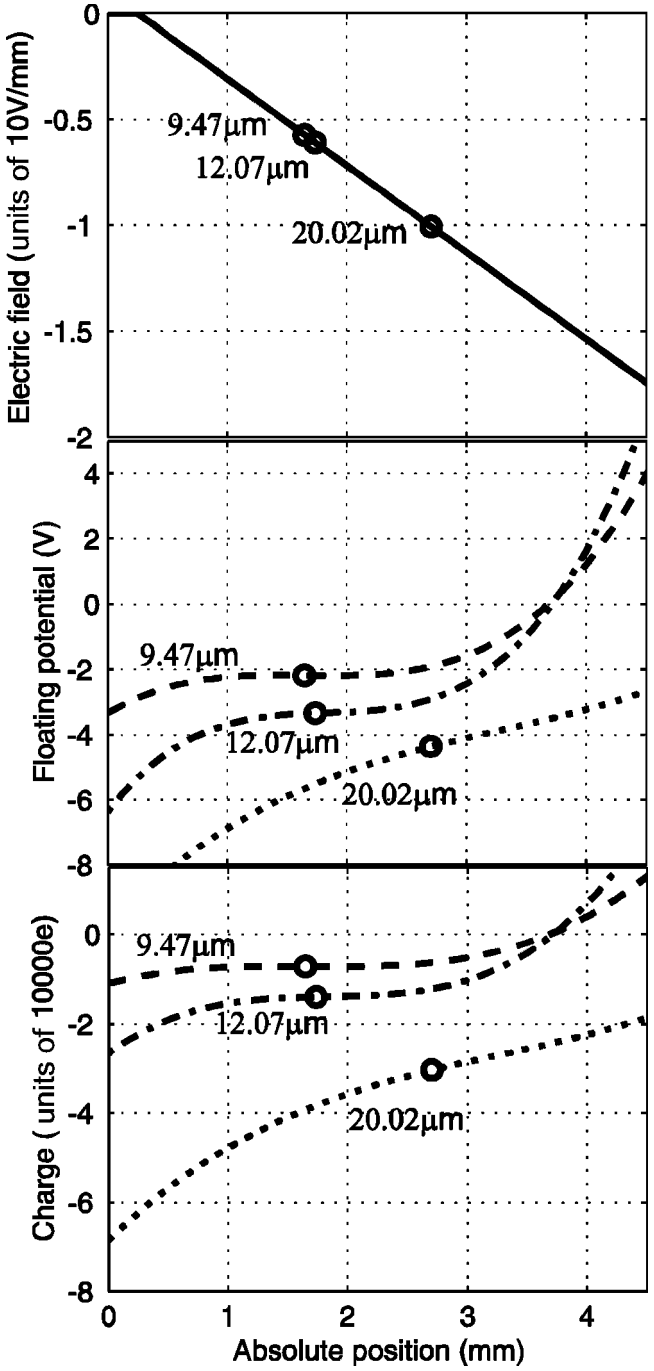

FIG. 5. Electric field, floating potential and charge components in the ''absolute coordinate system'' and particle equilibrium positions. The symbols mark the positions where the force balance is fulfilled for each particle.

The depth x_s was chosen in order to obtain the best agreement of the floating potential curves for all three particles. It was found to be $x_s = 0.25$ mm, in good agreement with Lieberman model, as can be observed in Fig. 2.

Assuming a linearly increasing electric field with a small plateau at the plasma edge and a polynomial-like variation of the charge on the particulate, the charge, and the floating potential are computed, using the values for C_1, C_2, and C_3 obtained above. They are plotted in Fig. 5.

TABLE II. Charge components in the ''absolute coordinate system.''

d (μm)	$\tilde{Q}_0$ (e)	$\tilde{Q}_1$ (e/m)	$\tilde{Q}_2$ (e/m^2)	$\tilde{Q}_3$ (e/m^3)
9.47	1.10×10^4	-7.18×10^6	4.42×10^9	-8.92×10^{11}
12.07	2.67×10^4	-1.98×10^7	1.06×10^{10}	-1.93×10^{12}
20.02	6.86×10^4	-2.64×10^7	6.24×10^9	-6.34×10^{11}

The values for the charge components are given in Table II. The electric field slope is defined by $\tilde{E}_1 = 4.10 \times 10^6$ V/m^2. It was obtained from the potential drop between the quasineutral plasma ($V_{plasma} = 32.5$ V) and the electrode self-bias ($V_{bias} = -45.7$ V)

$$\int_{x_s}^{x_{max}} E(X)dX = V_{plasma} - V_{bias}. \tag{24}$$

Figure 6 shows the particle charge at the equilibrium position as a function of particle radius. It can be easily observed that the charge is not a linear function of the radius.

Recently, in similar experiments, Ivlev *et al.* [10] have studied experimentally nonlinear oscillations of microspheres. They determined the coefficients of nonlinearity from super-harmonic and subharmonic resonances that do not occur under our experimental conditions. They attributed the nonlinearity completely to the electric field, treating the dust charge as constant. Applying this model to our data, the electric field components E_1, E_2, E_3 were computed. The so determined electric field is shown in Fig. 7. The curves show that the electric field is extremely nonlinear. Furthermore, the electric field computed for the 9.47 μm and 12.07 μm becomes positive deeper in the sheath. This is in contradiction with the statements of Lieberman model. Thus, a model of spatially constant dust charge is not in agreement with our experimental data.

Therefore in following step, a spatially variable charge of the particle and a nonlinear electric field were taken into account. The electric charge on the grain surface is still considered to be described by a third order polynomial whereas the electric field is considered to be parabolic.

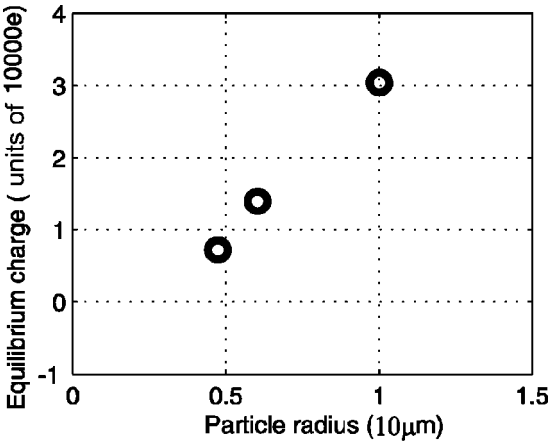

FIG. 6. Particle charge at the equilibrium position.

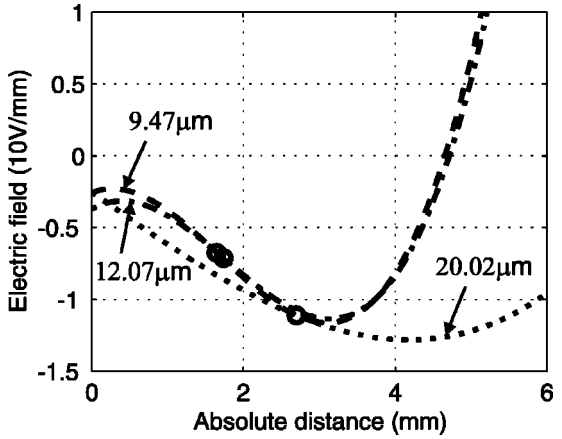

FIG. 7. Electric field components assuming a constant charge of the particle over the whole sheath. The symbols mark the positions where the force balance is fulfilled for each particle.

$$E(X)=\begin{cases}0, & X\leqslant x_s\\ \tilde{E}_1(X-x_s)+\tilde{E}_2(X-x_s)^2, & X>x_s.\end{cases} \tag{25}$$

Again the values for $\tilde{E}_1$ and $\tilde{E}_2$ have to satisfy the potential drop condition according to Eq. (24). The electric field and floating potential for all three particle sizes are plotted in Fig. 8 for three representative sets of values for the electric field components $\tilde{E}_1$ and $\tilde{E}_2$. $\tilde{E}_1$ is chosen as arbitrarily between 0 and 4×10^6 V/m^2 and $\tilde{E}_2$ is computed using Eq. (24). For larger values of E_1, E_2 would become negative, resulting in an unphysical concave curvature of the electric field. As it can be observed, the floating potential curves corresponding to the largest particle are still shifted from the curves corresponding to the smaller particles, for each set of electric field components. Figure 8(c) with $\tilde{E}_1=4\times10^6$ V/m^2 nearly corresponds to the case of linear electric field discussed above.

VI. DISCUSSION

All three curves representing the electric charge of the particles show the same general trend of the negative charge to decrease with increasing depth in the plasma sheath. This is mainly due to the reduction of electron density in the sheath that leads to a less effective charging of the particle [see Fig. 2(a) and Eq. (11)]. The experiments support this finding. The change of the asymmetry coefficient C_2 can be related to the change of slope of the floating potential curve. The weakening of the potential curves, as seen in the experimental resonance curves, can be traced back to a negative C_3 and thus to the curvature of the floating potential curve, as found in the model.

A quite good mutual overlapping of floating potential curves was obtained for 9.47 μm and 12.07 μm, either assuming a linearly increasing or for a nonlinear electric field, but, in both cases, the curve corresponding to the 20.02 μm particle is somewhat shifted.

This leaves some question marks on the capacitive charging model assumed for the particle. According to Tomme *et al.* [8], the charge is not a simple linear function of the particle radius, but has a more complicated, nonlinear dependence. This is the reason why we consider that the simple capacitive model is not able to totally explain the charging process for all particle sizes and/or for all regions of the plasma sheath.

The comparison with results of Ref. [8] shows a good agreement for the light particles (9.47 and 12.07 μm), while for the heavier particle (20.02 μm), the agreement is worse.

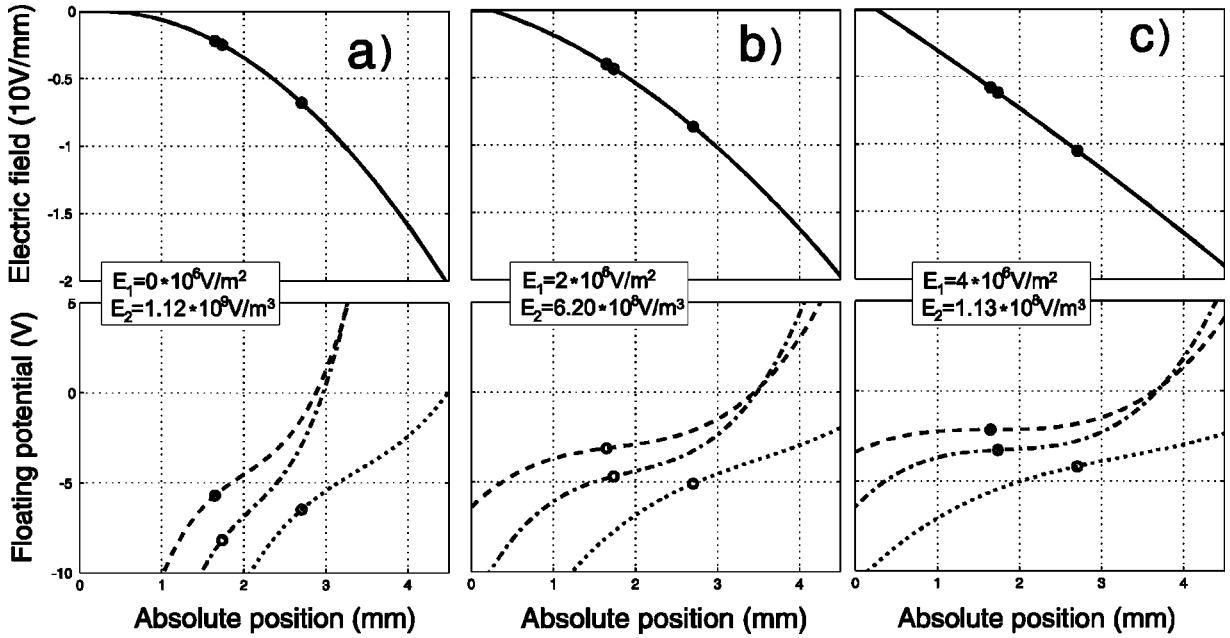

FIG. 8. Electric field and floating potential, assuming a nonlinear charge of the particle and a parabolic electric field in the sheath. The symbols mark the positions where the force balance is fulfilled for each particle.

The main reason is that this model starts with different assumptions (a constant charge of the particle over the whole oscillation amplitude and another kind of oscillation studied there, i.e. damped oscillations of dropped particles).

On the other hand, another effect can influence the charging of the particle. As it was shown in Sec. V, the heaviest particles float about 3 mm deep in the sheath. If we compare this depth with the mean free path of ion-neutral collisions computed at the experimental pressure and ion drift velocity, the values are quite close (the mean free path is about 3.8 mm). Considering this, an altered ion current at the particle position, due to the charge transfer and elastic collisions in the sheath, is to be taken into account. This alters the ionic current given in the OML model, leading to a less efficient ion decharging of the particle and to a higher negative charge on the dust grain than predicted by the OML model.

Another source of uncertainty is that the largest particles are made of a different material than the smaller ones. Since at the microscopic scale, the way that charges stick to the polymer chains of the material is not known in detail, a different charging might occur for different materials.

VII. CONCLUSIONS

Here, experimental results on particle oscillations in a capacitive rf plasma have been presented. Previous experiments relied on a constant charge of the particle and a linearly increasing electric field in the plasma sheath. Here we extended the model to a position dependent charge and a nonlinearly increasing electric field to explain the nonlinear resonances by introducing higher order terms into the general equation of motion. The nonlinear resonances have been attributed to an anharmonic potential energy well with up-down asymmetry and weakening at higher oscillation amplitudes.

The charging function components corresponding to one set of experimental conditions were computed, for three different particle sizes, putting the charging model in agreement with the experimental data.

Both linearly increasing and nonlinear electric fields were taken into account for computing the charge components and the floating potential. Thus it was demonstrated that the simple capacitance model cannot explain the charging behavior of all three particles. Overall good agreement with the experimental data and with the theoretical model of the plasma sheath is found for the linearly increasing electric field.

ACKNOWLEDGMENT

This work was supported by DFG Grant Nos. Pi185-17/1 and INTAS 97-0775.

[1] H. Ikezi, Phys. Fluids **29**, 1764 (1986).
[2] H. Thomas, G. E. Morfill, V. Demmel, J. Goree, B. Feuerbacher, and D. Möhlmann, Phys. Rev. Lett. **73**, 652 (1994).
[3] J. H. Chu and I. Lin, Phys. Rev. Lett. **72**, 4009 (1994).
[4] Y. Hayashi and K. Tachibana, Jpn. J. Appl. Phys., Part 2 **33**, L804 (1994).
[5] A. Melzer, T. Trottenberg, and A. Piel, Phys. Lett. A **191**, 301 (1994).
[6] A. Homann, A. Melzer, and A. Piel, Phys. Rev. E **59**, 3835 (1999).
[7] H. Schollmeyer, A. Melzer, A. Homann, and A. Piel, Phys. Plasmas **6**, 2693 (1999).
[8] E. B. Tomme, B. M. Annaratone, and J. E. Allen, Plasma Sources Sci. Technol. **9**, 87 (2000).
[9] T. Trottenberg, A. Melzer, and A. Piel, Plasma Sources Sci. Technol. **4**, 450 (1995).
[10] A. V. Ivlev, R. Stterlin, V. Steinberg, M. Zuzic, and G. Morfill, Phys. Rev. Lett. **85**, 4060 (2000).
[11] S. Nunomura, T. Misawa, N. Ohno, and S. Takamura, Phys. Rev. Lett. **83**, 1970 (1999).
[12] P. S. Epstein, Phys. Rev. **23**, 710 (1924).
[13] T. Nitter, Plasma Sources Sci. Technol. **5**, 93 (1996). In this reference the ion current equation (27) has a misprint. Here the correct equation is used.
[14] M. A. Lieberman, IEEE Trans. Plasma Sci. **PS-16**, 638 (1988).
[15] E. B. Tomme, D. A. Law, B. M. Annaratone, and J. E. Allen, Phys. Rev. Lett. **85**, 2518 (2000).
[16] C. Hayashi, *Nonlinear Oscillations in Physical Systems* (Princeton University Press, Princeton, NJ, 1985).